E.M. Godzhayev[2], S.Sh. Kakhramanov[1], K.J. Gulmamedov[2], A.Yu. Gamzayeva[3]

[1]Scientific-Production Association "Selen" of the NAS of Azerbaijan,
14, F. Agayev Str., Baku, 370143, Azerbaijan;
[2]Azerbaijan Technical University, 25, Huseyn Javid Ave.,
Baku, AZ1073, Republic Azerbaijan;
[3]Gyandzha State University, 187, Shah Ismail Xetai,
Gyandzha, AZ2000, Azerbaijan

SURFACE NANOPARTICLES IN $A^{V}{}_2B^{VI}{}_3$

Nanoparticles formed on (0001) $A^{V}{}_2B^{VI}{}_3$ surface are a specific class of nanoobjects affecting the properties of the bulk crystals. Their clustering in $Te^{(I)}$-$Te^{(I)}$ space occurs with aggregation of diffusing atoms according to the same mechanisms as in known solid-state structures formed on the free surface of crystals. Analysis of nanofragment structure and morphology conducted on the basis of AFM images and X-ray diffraction images on (0001) $A^{V}{}_2B^{VI}{}_3$ surface has revealed the role of van der Waals gap as a solid-phase nanoreactor during intercalation for Sb_2Te_3 <Cr> and (Bi_2Te_3-Bi_2Se_3) <ZnSe> solid solution.

Key words: *X*-ray diffraction image, diluted magnetic semiconductors, fractal clusters, nanoreactors.

Introduction

Looking for ways to improve the thermoelectric figure of merit of substances, apart from fundamental significance is also of applied importance for solving practical tasks of producing low temperatures by thermoelectric methods.

To this day it has been established that diluted magnetic semiconductors based on the elements of III and V or II and IV groups of periodic system pass into ferromagnetic state at low temperatures. Ferromagnetism was quite recently discovered in bismuth telluride with *Fe*, and then in antimony telluride with V at low temperatures. The influence of magnetic impurities on thermoEMF, resistance, magnetism, the Hall effect, the Shubnikov-de Haas effect and other properties of such crystals was discovered [1].

Study of materials with high thermoelectric figure of merit is of particular relevance today. Optimal parameter values are achieved by introducing various doping impurities. In so doing, to achieve high thermoelectric figure of merit, one should study the fundamental physical properties of materials.

As the doping impurities *Cr, Zn* can be used. However, to this date the effect of these impurities on the energy spectrum of $(Bi_{1-x}Sb_x)_2Te_3$ mixed crystals is poorly understood, no data is available on the thermoelectric figure of merit of diluted magnetic semiconductors based on antimony telluride and the effect of magnetic impurities on the oscillation properties of such crystals. There is no information on the thermoelectric properties of mixed $(Bi_{1-x}Sb_x)_2Te_3$ crystals doped with chromium. The Fermi surface anisotropy of *p*-$(Bi_{1-x}Sb_x)$ single crystals and Bi_2Te_3 type crystals has not been determined by direct methods.

In this work, three types of samples were investigated.

The first type is mixed single crystals of bismuth and antimony tellurides, both undoped and doped. The second type is single crystals of antimony telluride doped with chromium magnetic impurity. Samples of the third type are single crystals of iron doped single crystals of bismuth telluride and selenide.

In [1], systematic study of the effect of chromium doping on galvanomagnetic, thermoelectric, oscillation and magnetic properties of layered Sb_2Te_3 single crystals was performed in the temperature range of 1.7 – 300 K. The Fermi surface anisotropy was determined by direct measurements of the angular dependences of the Fermi surface extreme sections with the aid of the Shubnikov-de Haas effect of $(Bi_{0.5}Sb_{0.5})_2Te_3$ single crystals.

The totality of data on the influence of doping with gallium, chromium and iron on thermoEMF, galvanomagnetic properties and energy spectrum is necessary for the optimization of devices and instruments based on bismuth and antimony tellurides. The use of investigated impurities *Ga*, *Cr*, *Fe* increases thermoEMF, and magnetic impurities *Cr*, *Fe*, *Ga* can be used for creation of new solid-state devices with magnetic field control. The results of research results can serve the basis for the development of a promising technology of producing materials with assigned properties on the basis of semiconductors of bismuth and antimony telluride types.

In [2], approaches to synthesis of nanocomposites based on zero-, one- and two- dimensional solid-state nanoreactors formed by zeolite cavities or interlayer voids of layered compounds are considered.

Bi_2Te_3 nanowires were obtained in the matrix of porous aluminum oxide [3]. However, in Bi_2Te_3 itself, as a result of crystallization, nanosized particles are formed in the interlayers of superstoichiometric atoms [4], and fractal structures are analyzed in terms of physics of fractal clusters. They are formed during nanoislands growth process with adhesion of solid particles [5-6]. Surface morphology study of (0001) Bi_2Te_3 <impurity> and consideration of interlayer aggregates with observed nanolayer assemblies [6] required to clarify the influence of self-organized nanoparticles based on impurities between $Te^{(1)}$-$Te^{(1)}$ $A^{V}{}_2B^{VI}{}_3$ on thermoelectric properties.

This called for new experimental data on studying the surface morphology of (0001) $A^{V}{}_2B^{VI}{}_3$ doped with metals (*Zn*, *Se*, *Cr*).

In the light of the foregoing, the following purpose can be formulated: using *X*-ray diffraction and atomic force microscopy methods, to determine the composition of resulting intercalated interlayer nanofragments, using $Te^{(1)}$-$Te^{(1)}$ $A^{V}{}_2B^{VI}{}_3$ space as a nanoreactor.

1. Experiment and results

Bi_2Te_3 compound was prepared by thermal synthesis at 900 – 950 K, which was generally carried out in quartz ampoules where *Bi, Te* and impurities were loaded in proper ratio. The synthesized alloys were loaded into graphitized ampoules (diameter 8 mm), alloyed again and then, vertical directional crystallization was used to get single-crystal ingots with temperature gradient ΔT = 120 degrees/cm and crystallization rate 1.4 cm/h. In such crystals, after cleaving along (0001) Bi_2Te_3 plane, the morphology of impurity nanoparticles was studied. Structurally, such samples can be considered as intercalation ones, since one can single out the layers of host array and guest (impurities) in them. Because of a weak chemical bond between $T_e^{(1)}$-$T_e^{(1)}$ a change in morphology of interlayer space with penetration of metal atoms and formation of semiconductor nanoparticles is typical here.

Intercalation of *Zn* and *Cr* atoms was performed at 600 K. For this purpose, thermal technique was used to evaporate metals on purified surface along basis plane (0001) onto sample end face. Later the process of intercalation along (0001) layers was conducted at temperature gradient ΔT = 50 degrees/cm, the evaporated part of the sample serving the hot side. On the samples obtained by this method the as-cleaved (0001) surfaces were investigated and the electron microscopic images and *X*-ray diffraction patterns were analyzed.

1.1. AFM and XRD studies

Electron microscopic images were obtained on NC-AFM atomic force microscope. *X*-ray diffraction studies were carried out on Philips Panalytical installation (*X*-ray difractometer). Preparation of pure surface by cleavage with special tools was done along (0001) basis plane in the air immediately prior to conducting the experiments.

For all doped samples, apart from 3D AFM images of (0001) $A^{V}{}_2B^{VI}{}_3$ surface, there were investigated 2D AFM images, the distribution functions of equal-size nanoparticles, the density of distribution of nanofractals on (0001) surface along the height.

Nanoislands of nanosize 5 – 10 nm, assumed to be nanoparticles, were obtained in Sb_2Te_3<*Cr*>, Bi_2Te_3<*Cr*>, Bi_2Se_3<*Se*> single crystals between $Te^{(1)}$-$Te^{(1)}$ layers.

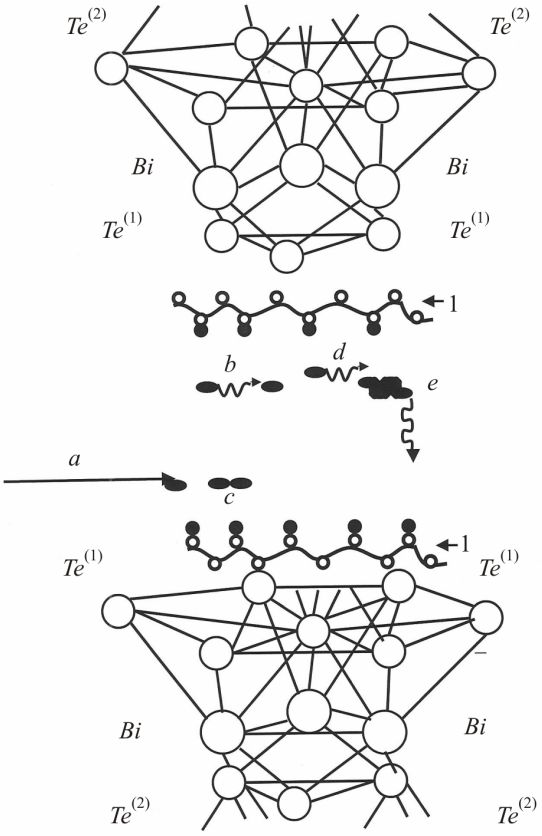

Fig. 1. Schematic of arrangement of bismuth and telluride atoms in Bi_2Te_3 structure, model approximations of nanoparticles between $Te^{(1)}$-$Te^{(1)}$ at intercalation of easily diffusible impurities into interlayers: a – atom inclusions along (0001)plane; b – formation of a new island; b and d – diffusion of particles; c – aggregation; e – island diffusion; 1 – aggregation of particles between $Te^{(1)}$-$Te^{(1)}$.

In $A^{V}{}_2B^{VI}{}_3$ the guest atoms (*ZnSe, Cr*) are localized in van der Waals space between telluride quintets. A quintet consists of five simple layers. Atoms of individual layer are identical and form a plane hexagonal lattice. Atoms of each subsequent layer are arranged above the centres of triangles formed by the atoms of previous layer. $T_e^{(1)}$ atoms have as the nearest neighbours six *Bi* atoms, three from each adjacent layer. On the one side $T_e^{(1)}$ is bound with three *Bi* atoms, and on the other side – with three $T_e^{(1)}$ atoms, i.e. in the lattice there are two essentially different places for *Te* atoms [4]. Fig. 1 shows a schematic of atoms arrangement in Bi_2Te_3 crystal lattice, the ways of diffusion (marked by arrow (*a*)) and aggregation of particles between telluride quintets (*b*, *e*, *c*) leading to formation of nanolayers (1). The distance between the quintets is relatively large, i.e. $T_e^{(1)}$-$T_e^{(1)}$ bond is very weak.

The most probable places for accumulation and nucleation of nanoparticles based on *Zn, Cr, Fe* can be *Te* vacancies, sets of the type "dislocations-impurity atom", the boundaries of blocks and grains, microcracks and concentration inhomogeneities [7-10].

Let us give the experimental data by the example of Sb_2Te_3<*Cr*>, Bi_2Te_3<*Cr*>, Bi_2Se_3<*Se*>. AFM images of nanoparticles formed on (0001) surface at chromium intercalation and synthesis of bismuth telluride together with *Cr* with subsequent crystallization are seen in Figs. 2 and 3. With intercalation at a temperature of 600 K chromium is introduced to the interlayers, like in nanoreactor interacting with superstoichiometric Sb_2Te_3 components: tellurium and antimony. This is testified by *X*-ray diffraction peaks from *CrSb*, *CrTe* nanoparticles. *X*-ray diffraction patterns (Fig. 4) of intercalated Sb_2Te_3<*Cr*> samples (obtained in the process of crystal growth) show peaks mainly from *CrSb* nanoparticles at $2\Theta = 44°$, 52°, 54° and 74°, and in *CrTe* at $2\Theta = 54°$ and the nanoislands of Sb_2Te_3 itself. Here, $T_e^{(1)}$-$T_e^{(1)}$ space serves not only as a nanoreactor, but as a nanocontainer for chromium (Fig. 4).

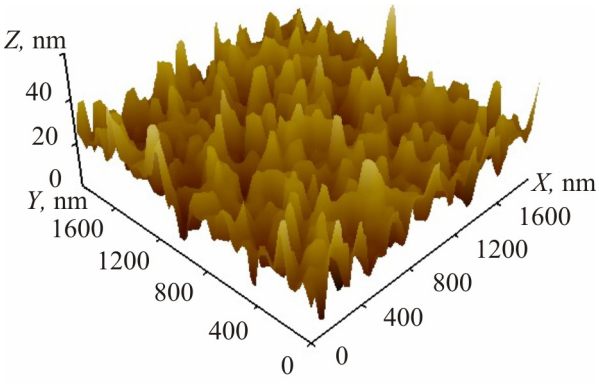

Fig. 2. 3D AFM image of (0001) surface of Cr-intercalated antimony telluride.

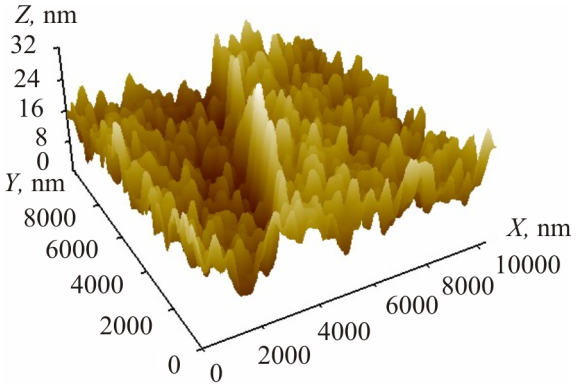

Fig. 3. 3D AFM image of (0001) surface of intercalated Bi_2Te_3<Cr>.

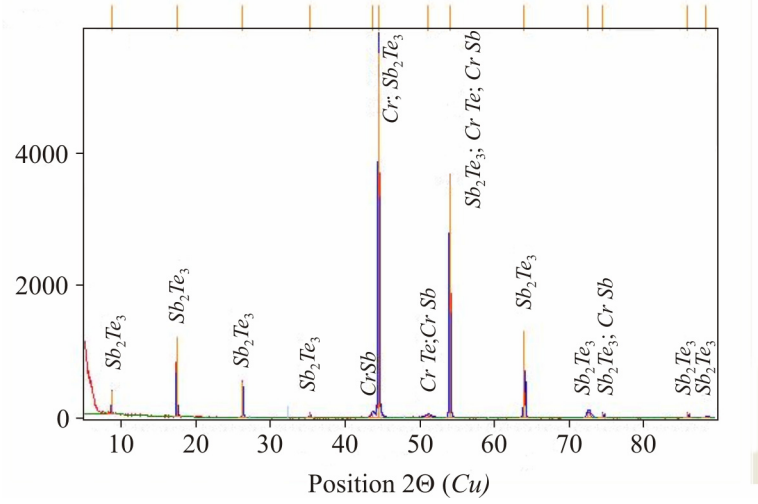

Fig. 4. X-ray diffraction image of (0001) surface of Cr doped Sb_2Te_3<Cr>.

Surface morphology of (0001) Sb_2Te_3<*Cr*> in 3D scale with *Cr* intercalation is represented in Fig. 2; nanoislands here consist of *CrSb, CrTe*. Here one can observe traces of *Cr* and Sb_2Te_3; the height of nanoislands varies from 5 to 20 nm. AFM image of Bi_2Te_3<*Cr*> shows nanoobjects of smaller size to 15 nm.

X-ray diffractometry for Bi_2Te_3<*Cr*> is given in Fig. 5: here, $Te^{(1)}$-$Te^{(1)}$ medium was a nanocontainer

for *Cr*: (2Θ = 43°, 51°). *X*-ray diffraction images for Bi_2Se_3<*Se*> are shown in Fig. 6, and for *n*-type <*ZnSe*> solid solution in Fig. 7; *X*-ray diffraction peaks are mainly seen from *ZnSe* at 2Θ = 45°, 73° and 74°. In Bi_2Se_3 van der Waals gap serves not only as a nanocontainer, but also as a nanoreactor.

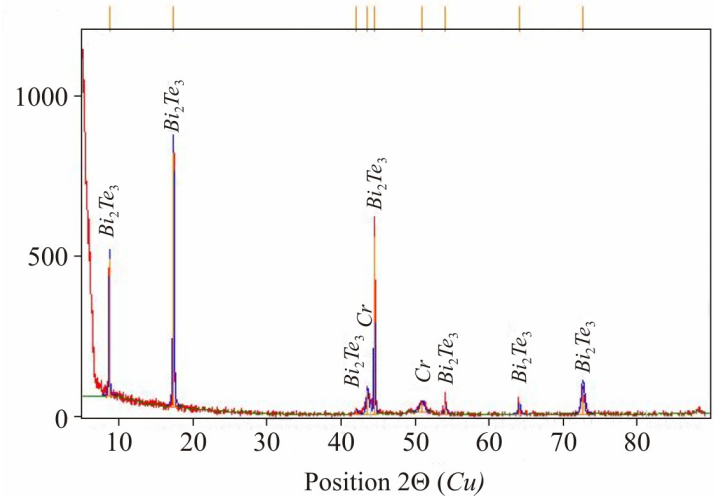

Fig. 5. 3D X-ray diffraction image of (0001) Bi_2Te_3<Cr> surface.

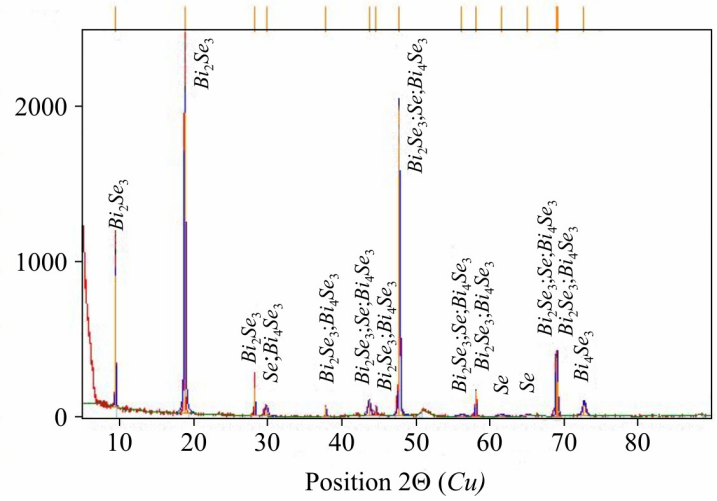

Fig. 6. X-ray diffraction image of fractal surfaces in Bi_2Se_3<Se> system.

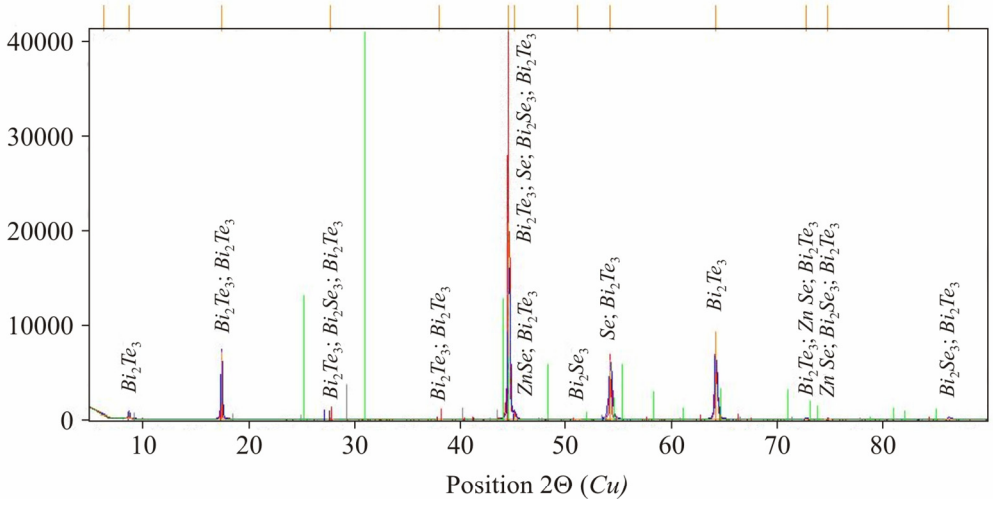

Fig. 7. X-ray diffraction image of (0001) in (Bi_2Se_3·4mol %-Bi_2Te_3 96 mol %) <ZnSe> solid solution.

1.2. Mechanism of atoms diffusion and their aggregation

Supposed ways of particles diffusion and their aggregation with subsequent formation of nanoislands (Fig. 1) most probably are related to the process of filling with impurities of places around the dislocation wells and *Te* vacancies on the interlayer surface (0001) $A_2{}^{V}B_3{}^{VI}$. The onset of nanocells formation takes place in the process of impurities diffusion along the basis plane (0001) and their growth from the surface on *Te* vacancies and telluride quintets. Interacting and touching one another, nanoislands are formed on the basis plane (0001), which is evidently reflected on their topography. The process of coagulation reaches its peak whereby the nanoislands which are formed create a single nanofractal surface consisting of chromium which we observe in Fig. 3 for Bi_2Te_3<*Cr*>system.

Similar AFM surfaces between $T_e^{(1)}$-$T_e^{(1)}$ $A_2{}^{V}B_3{}^{VI}$ were obtained for Bi_2Se_3<*Se*> (see 8), as well as for solid solution (Bi_2Te_3 96 mol %-Bi_2Se_3 4 mol%) <*ZnSe*> (Fig. 9).

Almost all steps of van der Waals zone filling are related to the process of quick introduction of easily diffusible impurities (*Zn, Cr* and *Se*) into $A_2{}^{V}B_3{}^{VI}$ along the basis plane as a result of diffusion directions (direction (*a*) in Fig. 1).

Nanoislands of fractal nature grow from nucleation center on telluride vacancies. Walking at random, *Zn, Cr* atoms move along the basis plane (0001) as a result of gradient diffusion. Contacting with the nucleus of a primary island, moving impurity atoms adhere to it. Then from a new point in the space between $T_e^{(1)}$-$T_e^{(1)}$ another atom starts to move, randomly walking and again contacting with another nanoobject, increasing its size.

The size of interlayer space $T_e^{(1)}$-$T_e^{(1)}$ in Bi_2Te_3 ~ 3 nm, the height of nanoparticles varies within 10 to 20 nm. Here, reversible compression or tension of quintets is also possible. The distance $T_e^{(1)}$-$T_e^{(1)}$ can be smoothly controlled, tuning the nanoreactor under study for given volume by filling with impurities the interlayer space.

Nanoobjects in the studied systems were self-organized, and in (Bi_2Te_3-Bi_2Se_3) <*ZnSe*> solid solution they were accompanied by association of particles of close dimensions (for instance, Bi_2Se_3, *Se*, Bi_2Te_3 and *ZnSe*) – Fig. 9.

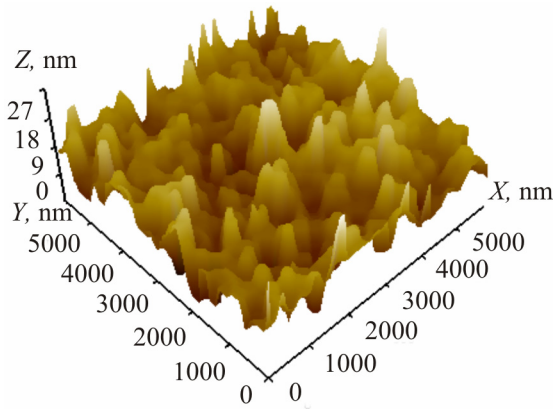

Fig. 8. 3D AFM image of (0001) Bi_2Se_3<Se> surface.

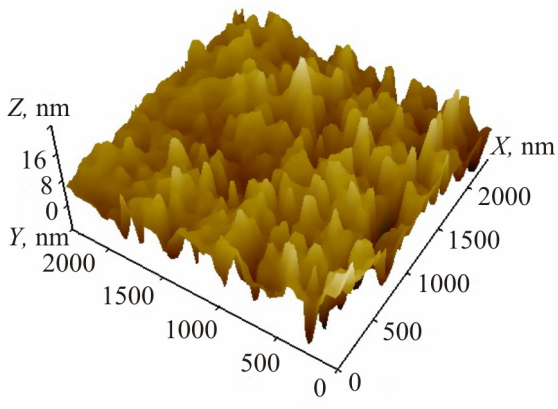

Fig. 9. 3D AFM image of (Bi_2Te_3 96 mol % – 4 mol %) <ZnSe>solid solution surface.

According to the geometrical sign of dimensionality the resulting nanoobjects have nanosizes in all three directions: their height does not exceed 15 to 20 nm, their width and length vary within lower than 100 nm limits; i.e. in conformity with classification [2] these nanoobjects can be referred to nanoparticles with a disordered distribution. However, in (0001) surface morphology one can see nanoislands of smaller size ~ 5 to 10 nm that can be referred to clusters. As we see, nanoformations form a part of interlayer structure in doped $A^{V}{}_2B^{VI}{}_3$. In our opinion, they affect the anomalous Hall effect and

ferromagnetism in the systems that we investigated. We will now consider the physical characteristics of Sb_2Te_3, Bi_2Te_3 and their solid solutions that are strongly affected by chromium atoms.

1.3. Thermoelectric figure of merit in solid solutions [8]

In *p*-type solid solutions based on bismuth and antimony chalcogenides *p*-$(Bi, Sb)_2$ $(Te, Se)_3$ the peculiarities of change in thermoelectric figure of merit (Z) were analyzed with regard to data obtained in the investigation of thermoelectric and galvanomagnetic properties. It is shown that in samples with optimal charge concentrations for the temperature range of 300 to 370 K in a multicomponent composition $p\text{-}Bi_{2-x}Sb_xTe_{3-y}Se_y$ ($x = 1.3$, $y = 0.06$) Z is determined by high mobility and low lattice thermal conductivity. Increase in the density of states effective mass and increase in the slopes of temperature dependence of mobility as compared to other compositions lead to Z increase in $p\text{-}Bi_2Sb_xTe_3$ solid solution at $x = 1.6$ in the temperature range of 370 – 550 K.

Increase in thermoelectric figure of merit in compositions under study is also determined by increase in compression of constant energy ellipsoids along the binary and bisector directions and by change in angle θ between the principal axes of ellipsoids and crystallographic axes [8].

The effect of suppression of intrinsic conduction in a narrow-gap semiconductor $p\text{-}Bi_{0.5}Sb_{1.5}Te_3$ by plastic deformation has been established. The effect becomes apparent in the attenuation of the Seebeck coefficient reduction at elevated temperatures due to intrinsic conduction. This effect can be caused by increased disorientation of crystal grains, formation of small-size nanoparticles leading to reduction of thermal conductivity and mobility of preferably interlayer charge carriers.

1.4. Anomalous Hall effect in $Sb_{2-x}Cr_xTe_3$

Layered semiconductor structures with nanoislands are characterized by a series of phenomena and properties that are of interest for the pursuance of the research and attractive in thermoelements.

Semiconductors of Sb_2Te_3 type have a rhombohedral structure (space group of symmetry $R3m$ – $D^5{}_{3d}$) with dyad axes C_2 and triad axes C_3. Sb_2Te_3 crystals are always *p*-type due to high concentration of point charged defects of preferably anti-structural type, that is, antimony atoms occupy tellurium positions. The reason for such defects formation is a weak polarity of *Sb-Te* bonds. At liquid helium temperature the observed negative magnetoresistance and anomalous Hall effect, in our opinion, are related to the influence of nanoparticles formed in the medium of $Te^{(1)}\text{-}Te^{(1)}$ $A_2{}^{V}B_3{}^{VI}$ (see Fig. 2).

The Hall coefficient in all the samples is positive and increases with increasing chromium content, which points to holes concentration reduction. However, it does not seem possible to use it for the calculation of holes concentration, since in bismuth and antimony tellurides there are two groups of holes with different concentrations and mobilities that are unknown.

Thus, we see that van der Waals gap is a peculiar kind of nanoreactor, where nucleation of quasi-two-dimensional layers with nanoislands between $Te^{(1)}\text{-}Te^{(1)}$ takes place on the surface (0001) (Sb_2Te_3) Bi_2Te_3<impurity>. These structural voids – nanoreactors – are filled with compounds whose further modification leads to formation of (*CrSb*) nanoparticles. Formed by $Te^{(1)}\text{-}Te^{(1)}$ cavities of layered crystals, nanoreactors open up wide opportunities for the design of nanocomposites with given thermoelectric properties.

Study of surface morphology of (0001) Sb_2Te_3 and its solid solution $Bi_{1.2}Sb_{4.8}Te_9$<*Te*> by electron microscopy and *X*-ray diffractometry methods has shown that atoms which did not react with other elements can also settle in the van der Waals gap $Te^{(I)}\text{-}Te^{(I)}$ (see Fig. 3). Conditions of formation in the interlayers-nanoreactors lead to the emergence of small-size nanoparticles. However, these results call for further research that will be published in our subsequent publications.

Paper [11] presents analysis of problems and approaches to their solving for semiconductor nanostructures with quantum dots as applied to interlayer nanoobjects in hand, as well as our data on the uniformity of nanoislands in their ensemble on the van der Waals surface (0001) $A^{V}{}_2B^{VI}{}_3$ <impurity>. In a compact array of nanoislands the imposition of elastic strain fields is possible, which creates effects that cause changes in the electron properties of nanostructured crystals. Problems whose solution calls for further efforts can be listed as follows: first, enhancement of size uniformity of nanoobjects array (see Figs. 2, 3 and 8, 9) with retention of a single shape and their elemental composition; second, control of space arrangement (space-ordered arrays) suitable for getting maximum compact and sparse arrays; third, reduction of the density of extended (dislocations) and point defects. Of particular interest are nanoparticles of small size (≤ 100 nm) as artificial atoms with a small number of bound states characterized by the value of energy gap between discrete levels, assuring the operation of devices at temperatures 100 to 350 K.

Let us compare the ATM images that we obtained in Fig. 9 to investigations [12] in percolation cluster of *ZnSe* quantum dots as a fractal object.

Of big importance are the results of studying samples with *ZnSe* quantum dots with the density corresponding to percolation threshold of excitons and much in excess, when quantum dots form conglomerates [12]. For the first time, emission of excitons from the percolation cluster of bound quantum dots as a fractal object was discovered. Structural analysis of photoluminescence spectra of samples has shown that they are determined by the contribution of exciton states located in different structural elements of percolation cluster, such as backbone (spine), dead ends and internal voids. The resulting percolation cluster of bound particles assures spreading the wave function of carriers for a microscopic distance. Percolation cluster is based on the so-called geometric or quantum percolation.

Experiments on the conductivity of samples allow establishing the moment of emergence of a percolation cluster of bound metal particles, but they cannot yield any information on the structure of percolation cluster, i.e. on its backbone, dead ends and internal voids. Percolation cluster is known to be a fractal object, so it cannot be uniform and continuous. The resulting AFM images (Fig. 9) can be referred to percolation clusters obtained above the percolation threshold. Further studies will be required in order to obtain on Bi_2Te_3 surface nanoobjects of *ZnSe* with distribution density below the percolation threshold.

Conclusions

Analysis of surface morphology of (0001) Bi_2Te_3 <*Cr, ZnSe*> has shown that nanoparticles are formed between $T_e^{(1)}$-$T_e^{(1)}$ layers both in nanoreactor and nanocontainer.

The reason for quick growth of nanofractal "islands" is apparently that *ZnSe, Cr* come from vacancies to telluride quintets.

Interlayer impurities interact with formation of nanofragments of *CrSb*, *CrTe* and *ZnSe*.

Thus, between $A_2{}^{V}B_3{}^{VI}$ quintets, nanoparticles of size 5 to 10 nm are self-organized in nanoreactor of only *CrSb* and *ZnSe*, and in Bi_2Se_3<*Se*> system, in the interlayers, nanoparticles are self-organized of Bi_4Se_3.

References

1. P.M. Tarasov, Thermoelectric, Galvanomagnetic and Magnetic Properties of Doped $(Bi_{1-x}Sb_x)_2Te_3$ Single Crystals, *Author's Abstract of PhD Thesis* (M.V. Lomonosov Moscow State University, 2009), p. 21.

2. Yu.D. Tretyakov, A.V. Lukashin, and A.A. Yeliseev, Synthesis of Functional Nanocomposites on the Basis of Solid-Phase Nanoreactors, *Russian Chemical Reviews* **73** (9), 974-998 (2004).
3. O. Rabin, P.R. Herz, S.B. Cronin, L. Lin, A.I. Akinwande, and M.S. Dresselhaus, *Mater. Res. Soc. Symp. Proc.* **637**, 4.7.1 (2001)
4. K. Aleskerov, S.Sh. Kakhramanov, E.M. Derun, M.G. Pishkin, and G. Kavei, Some Peculiarities of Nanoobjects Formations in the Interlayer Space of Bi_2Te_3 Type Crystals, *Azerbaijan J. of Physics* XII (4), 41-45 (2007).
5. B.M. Smirnov, *Physics of Fractal Clusters* (Moscow: Nauka, 1991), p. 134.
6. Jens Feder, *Fractals* (New York: Plenum Press, 1989), p. 250
7. I.V. Gasenkova, T.E. Svechnikova, Research on the Structure of Single Crystals of Solid Solutions Based on Bismuth Telluride, Proceedings of Interstate Workshop "Thermoelectrics and their Applications (2002), pp. 145-150.
8. L.N. Lukyanova, V.A. Kutasov, P.P. Konstantinov, and V.V. Popov, Thermoelectric Figure of Merit in *p*-type Solid Solutions Based on Bismuth and Antimony Chalcogenides at Above Room Temperatures, *Physics of the Solid State* **52** (8), 1492-1497 (2010).
9. B.M. Goltsman, V.A. Kutasov, and L.N. Lukyanova, Suppression of intrinsic conduction in p-$Bi_{0.5}Sb_{1.5}Te_3$ under plastic deformation *Physics of the Solid State* **50** (2), 235-236 (2008).
10. V.A. Kulbachinsky, P.M. Tarasov, and E. Bryuk, Anomalous Hall Effect and Ferromagnetism in a New Dilute Magnetic Semiconductor $Sb_{2-x}Cr_xTe_3$, *Letters to JETF* **81** (7), 426-430 (2005).
11. A.V. Dvurechensky, A.I. Yakimov, Physical Effects and Technologies as the Basis of Semiconductor Nanostructures with Quantum Dots for IR Range, *Izvestiya: Physics* **73** (1), 71-75 (2009).
12. N.V. Bondar, M.S. Brodin, Photoluminescence and Exciton Energy in Percolation Cluster of *ZnSe* Quantum Dots as the Fractal Object, *Semiconductors* **46** (5), 644-648 (2012).

Submitted 08.04.2013.